JCS ePress online publication date 21 June 2011

Galectin-3 maintains cell motility from the subventricular zone to the olfactory bulb

Isabelle Comte[1], Yongsoo Kim[1,2,*], Christopher C. Young[1], Judith M. van der Harg[1], Philip Hockberger[3], Paul J. Bolam[4], Françoise Poirier[5] and Francis G. Szele[1,‡]

[1]Department of Physiology, Anatomy and Genetics, University of Oxford, South Parks Road, Oxford OX1 3QX, UK
[2]Interdepartmental Neuroscience Program, Northwestern University, Chicago, IL 60611, USA
[3]Department of Physiology, Feinberg School of Medicine, Northwestern University, Chicago, IL 60611, USA
[4]MRC Anatomical Neuropharmacology Unit, Mansfield Road, Oxford OX1 3TH, UK
[5]Institut Jacques Monod, UMR CNRS 7592, Université Paris Diderot, 75205 Paris Cedex 13, France
*Present address: Cold Spring Harbor Laboratory, One Bungtown Road, Cold Spring Harbor, NY 11724, USA
‡Author for correspondence (Francis.Szele@dpag.ox.ac.uk)

Accepted 15 March 2011
Journal of Cell Science 124, 2438-2447

doi:10.1242/jcs.079954

Summary

The adult brain subventricular zone (SVZ) produces neuroblasts that migrate through the rostral migratory stream (RMS) to the olfactory bulb (OB) in a specialized niche. Galectin-3 (Gal-3) regulates proliferation and migration in cancer and is expressed by activated macrophages after brain injury. The function of Gal-3 in the normal brain is unknown, but we serendipitously found that it was expressed by ependymal cells and SVZ astrocytes in uninjured mice. Ependymal cilia establish chemotactic gradients and astrocytes form glial tubes, which combine to aid neuroblast migration. Whole-mount preparations and electron microscopy revealed that both ependymal cilia and SVZ astrocytes were disrupted in *Gal3*$^{-/-}$ mice. Interestingly, far fewer new BrdU^{+} neurons were found in the OB of *Gal3*$^{-/-}$ mice, than in wild-type mice 2 weeks after labeling. However, SVZ proliferation and cell death, as well as OB differentiation rates were unaltered. This suggested that decreased migration in vivo was sufficient to decrease the number of new OB neurons. Two-photon time-lapse microscopy in forebrain slices confirmed decreased migration; cells were slower and more exploratory in *Gal3*$^{-/-}$ mice. Gal-3 blocking antibodies decreased migration and dissociated neuroblast cell–cell contacts, whereas recombinant Gal-3 increased migration from explants. Finally, we showed that expression of phosphorylated epidermal growth factor receptor (EGFR) was increased in *Gal3*$^{-/-}$ mice. These results suggest that Gal-3 is important in SVZ neuroblast migration, possibly through an EGFR-based mechanism, and reveals a role for this lectin in the uninjured brain.

Key words: Subependymal zone, Rostral migratory stream, Neuroblast, Glia, Microglia, *Gal3*-null mutant mice

Introduction

Thousands of neurons are created every day in the subventricular zone (SVZ) of postnatal and adult mammalian brains (Petreanu and Alvarez-Buylla, 2002). In the SVZ, slowly proliferating astrocytes expressing glial fibrillary acidic protein (GFAP) give rise to rapidly dividing immature precursors that generate doublecortin (Dcx)-expressing neuroblasts. These neuroblasts migrate along a well-defined route: the rostral migratory stream (RMS) toward the olfactory bulb, where they differentiate into granular and periglomerular interneurons (Luskin, 1993). They advance in longitudinal chains, and are surrounded by astrocytic glial tubes (Peretto et al., 1997).

The SVZ and RMS contain a specialized molecular niche that promotes neurogenesis and migration. One of the niche factors with an important role in both proliferation and migration is post-translational glycosylation. Indeed, addition of polysialic acids to the neural cell adhesion molecule is crucial for SVZ cell motility (Ono et al., 1994). A complex mixture of proteins and carbohydrates regulates adhesion of the cells to the extracellular matrix (ECM). In addition, many proteins that are influential in SVZ migration, such as the epidermal growth factor receptor (EGFR), integrins, laminin and tenascin, are glycosylated (Kariya and Gu, 2009; Woodworth et al., 2004). However, much remains unclear about how these glycoconjugates and the molecules that mediate interactions between them regulate SVZ migration.

Galectins are a family of proteins (Gal-1 to Gal-15) identified by their similar carbohydrate recognition domains (CRDs), with a conserved sequence of approximately 130 amino acids that binds to galactoside residues. There are three different types of galectins, the proto-galectins which contain a single CRD and which can form homodimers, a chimeric galectin, characterized by a single CRD and a large N-terminal domain that contributes to self-aggregation, and the tandem-repeat galectins in which two CRDs occur within a single polypeptide and are bridged by a small peptide domain (Barondes et al., 1994; Hirabayashi and Kasai, 1993). Galectins regulate migration, cell–ECM adhesion, and cell survival depending on their intra- or extracellular localization (Elola et al., 2007). They have important actions in inflammation and cancer, but their potential functions in brain development and pathology are only now being revealed. It was recently discovered that Galectin-1 increases SVZ neurogenesis and improves recovery after stroke (Ishibashi et al., 2007; Sakaguchi et al., 2006), but the expression and function of other galectins in the SVZ is unknown.

Galectin-3 (Gal-3) is uniquely chimeric amongst galectins and has multiple roles (Delacour et al., 2009; Elola et al., 2007; Liu et al., 2002) including regulation of cell-ECM adhesion (Kuwabara and Liu, 1996) through laminin (Villa-Verde et al., 1995) and integrins (Takenaka et al., 2004). Gal-3 is also shuttled back and forth from the cytoplasm to the nucleus where it regulates pre-mRNA splicing (Haudek et al., 2010). Gal-3 becomes strongly

expressed in activated brain microglia in experimental autoimmune disease (Reichert and Rotshenker, 1999), prion infections (Mok et al., 2007) and after focal ischemia (Yan et al., 2009). In this study, we investigated the potential role of Gal-3 in normal adult brain and show that it is selectively expressed in the SVZ and RMS. By using *Gal3*(*Lgals3*)-null mice, function-blocking antibodies and recombinant Gal-3, we show that in contrast to Gal-1, it does not affect neurogenesis, but specifically regulates neuronal migration, and that loss of Gal-3 results in increased levels of phosphorylated EGFR.

Results

Gal-3 is expressed by a subset of SVZ cells

We first investigated the distribution of Gal-3 in the adult forebrain and found selective immunoreactivity in the SVZ and RMS (Fig. 1A). We confirmed specificity of the Gal-3 antibody by showing that no immunoreactivity was present in *Gal3*$^{-/-}$ mice (n=6). Gal-3 was not immunodetectable in the main OB granular and periglomerular layers, but was expressed in the accessory olfactory bulb (AOB) (Fig. 1A). We next determined which SVZ cell types expressed Gal-3 (Fig. 1B). Gal-3 immunoreactivity was punctate and diffuse. It formed a dense network surrounding clusters of PSA-NCAM$^+$ (polysialylated form of the neural cell adhesion molecule) neuroblasts (Rousselot et al., 1995), but was not expressed inside PSA-NCAM$^+$ chains (Fig. 1C). The Gal-3 expression pattern was reminiscent of the astrocyte tubes surrounding neuroblasts. Indeed, we found that Gal-3 immunofluorescence was associated with many glial fibrillary acidic protein (GFAP$^+$) SVZ astrocytes (Fig. 1D–F) and ependymal cells lining the lateral ventricles (Fig. 1F). Adult SVZ astrocytes and ependymal cells are derived from postnatal radial glia. Thus, in postnatal day 7 mice, it was not surprising to find Gal-3 immunoreactivity associated with vimentin$^+$ radial glia and astrocytes in the SVZ and RMS (supplementary material Fig. S1A–D). Using immunoelectron microscopy, we observed Gal-3$^+$ immunoprecipitates in both ependymal cells and astrocytes, confirming our previous results (Fig. 1G,H). Electron microscopy showed Gal-3 immunoprecipitates in the cytoplasm of ependymal cells and astrocytes, and also in the nuclei of a subset of astrocytes (Fig. 1G,H). We continued to characterize cell subtype Gal-3 expression with confocal light microscopy and found that a subset of Mash1$^+$ transit-amplifying progenitor cells contained Gal-3 immunofluorescence, primarily in the cytoplasm (Fig. 1I–K). Whereas activated CNS microglia express Gal-3 under pathological conditions (Walther et al., 2000) and CD45$^+$ SVZ microglial cells are constitutively semi-activated (Goings et al., 2006), most CD45$^+$ cells in the SVZ did not express Gal-3 (Fig. 1L–N). These results show that Gal-3 is selectively expressed in the SVZ in astrocyte-lineage cells and a subset of Mash1$^+$ precursors.

Gal3-null mice exhibit distorted SVZ cytoarchitecture

We used *Gal3*-null mice to investigate the role of Gal-3 in the SVZ and RMS. There was no significant change at the gross morphological level in brain length (WT, 14.9±0.3 mm; *Gal3*$^{-/-}$,

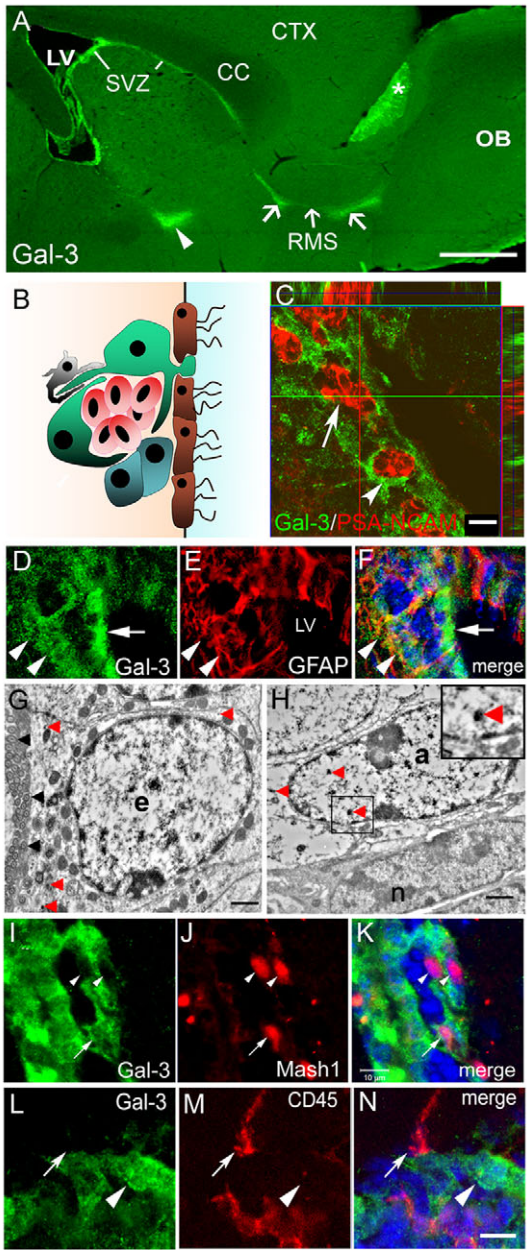

Fig. 1. Gal-3 expression on astrocyte lineage cells surrounds neuroblast chains. (**A**) Expression of Gal-3 in the SVZ, along the RMS (arrows) and in the accessory olfactory bulb (asterisk). Arrowhead indicates a portion of the ventral SVZ that was included in the sagittal section. CC, corpus callosum; CTX, cerebral cortex; LV, lateral ventricle; OB, olfactory bulb. Scale bar: 250 µm. (**B**) Cytoarchitecture of the SVZ. Astrocyte-like stem cells ('B cells', green) and transit-amplifying progenitor cells ('C cells', blue) surround migratory neuroblasts ('A cells', red). Microglia (grey) interdigitate cells and ciliated ependymal cells (brown) line the ventricle. (**C**) Confocal image shows Gal-3 (arrowhead) is not expressed by PSA-NCAM$^+$ neuroblasts (arrow), but Gal-3$^+$ cells surround neuroblasts. Scale bar: 10 µm. (**D–F**) Gal-3 immunofluorescence is diffuse and is associated with some GFAP$^+$ cells (arrowheads). Many ependymal cells also express Gal-3 (arrow). Blue in F is DAPI nuclear label. (**G**) Electron microscopy shows Gal-3 immunoreactivity (red arrowheads) in ependymal cell (e). Note the row of cilia (black arrowheads) on the left. Scale bar: 1 µm. (**H**) Gal-3 immunoprecipitates were observed in astrocytes (a) (arrowheads) but not in neuroblasts (n) using immunoelectron microscopy. Inset shows high magnification view of a Gal-3 immunoprecipitate. Scale bar: 1 µm. (**I–K**) Gal-3 (green) is expressed by few Mash1$^+$ cells (arrow) in the SVZ. Arrowheads indicate Mash1$^+$ cells that are Gal-3$^-$. Scale bar: 10 µm. (**L–N**) Gal-3 is rarely expressed by CD45$^+$ cells (red). Arrow shows close juxtaposition but lack of co-labeling. Arrowhead indicates a Gal-3$^+$ cell that is CD45$^-$. Scale bar: 10 µm.

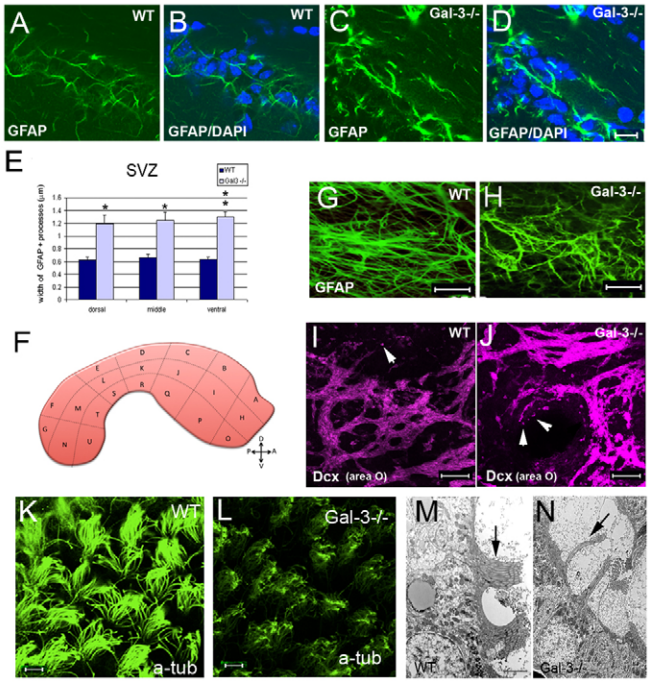

Fig. 2. Loss of Gal-3 disrupts SVZ cytoarchitecture. (**A**,**B**) The dorsal SVZ contains astrocytes with fine processes exhibiting moderate levels of GFAP immunofluorescence. (**C**,**D**) *Gal3*-null mice had increased levels of GFAP immunofluorescence, thickened processes, and overall distorted astrocytic morphology in the dorsal SVZ. (A–D) Coronal sectons. Photomicrographs in A–D were all taken with the same camera settings. Scale bar: 10 μm. (**E**) Quantification shows significant increases in the width of GFAP$^+$ processes in the dorsal, middle and ventral SVZ. *P<0.05; **P<0.005. (**F**) Schematic showing whole-mount dissection of the lateral ventricle wall and the subdivisions used for analysis. (**G**,**H**) Whole-mount immunohistochemistry showed that the normal orientation of GFAP$^+$ processes is disrupted in *Gal3*$^{-/-}$ mice. Scale bar: 20 μm. (**I**,**J**) Whole-mount immunohistochemistry shows that more Dcx$^+$ neuroblasts are migrating individually (arrowheads) in *Gal3*$^{-/-}$ mice compared with the control. *Gal3*$^{-/-}$ mice also had higher levels of Dcx immunofluorescence than WT in whole mounts. Scale bars: 20 μm. (**K**,**L**) Loss of cilia on ependymal cells in *Gal3*$^{-/-}$ mice is observed using anti-acetylated tubulin antibodies. Scale bar: 20 μm. (**M**,**N**) Electron microscopy also shows fewer ependymal cell cilia in *Gal3*$^{-/-}$ mice. Scale bar: 1 μm. All error bars represent s.e.m.

15.2±0.1 mm; P>0.5) or OB surface area (WT, 82,066±6239 μm^2; *Gal3*$^{-/-}$, 83,037±3780 μm^2, P>0.5). We also did not observe significant differences in the structure or size of the AOB in null mice (data not shown).

We examined the SVZ in detail and found increased GFAP immunoreactivity throughout the SVZ (Fig. 2A–D, supplementary material Fig. S2A–D) and RMS of *Gal3*$^{-/-}$ mice. GFAP$^+$ cell processes in the SVZ and RMS were distorted and appeared thicker than in wild-type. Indeed the width of GFAP immunostaining within astrocyte processes was significantly increased (Fig. 2E) in the dorsal SVZ (WT, 0.62±0.05; *Gal3*$^{-/-}$, 1.19±0.13 μm; P<0.05), middle SVZ (WT, 0.66±0.06; *Gal3*$^{-/-}$, 1.25±0.12 μm; P<0.01) and ventral SVZ (WT, 0.6±0.1; *Gal3*$^{-/-}$, 1.3±0.1 μm; P<0.001). GFAP immunoreactivity outside the SVZ and RMS was similar in all groups of mice. We next used whole-mount preparations of the lateral ventricular wall (Fig. 2F) and showed that the orientation of GFAP$^+$ processes was parallel to the LV wall in wild-type mice, but was disrupted in null mice (Fig. 2G,H). Next, we showed with whole-mount immunohistochemistry that Dcx immunostaining was increased in anteroventral subregions O and H (Fig. 2H) in null mice (Fig. 2I,J). The number of Dcx$^+$ neuroblasts migrating individually seemed to be increased in the entire lateral ventricle wall (Fig. 2J), suggesting that neuroblast migration was affected by the lack of Gal-3. Although the number of individually migrating cells appeared to be increased, the integrity of chains in *Gal3*$^{-/-}$ mice viewed in whole mounts (Fig. 2J) and with EM, was not altered (supplementary material Fig. S1E,F).

We examined cilia in the ependymal layer of Gal-3-knockout (KO) mice using acetylated tubulin as a marker, and showed remarkable loss of ciliary density (Fig. 2K,L, supplementary material Fig. S2C–H). This was confirmed with electron microscopy (Fig. 2M,N). Cilia are polarized to one side of ependymal cells; however, this ependymal planar cell polarity was not changed in null mice (supplementary material Fig. S2E,H). These data suggest that the absence of Gal-3 disrupts several aspects of SVZ and ependymal cell cytoarchitecture, which could cause an impairment of normal neuroblast migration.

Gal-3 is dispensable for SVZ proliferation and cell death

Gal-3 affects cell proliferation and apoptosis in several systems (Zhao et al., 2010). To investigate whether Gal-3 affects cell proliferation in the SVZ, we injected a single pulse of BrdU 2 hours before sacrifice (Fig. 3A). There was no significant difference in the number of BrdU$^+$ cells in the SVZ between control littermates and mutant mice (WT, 79.0±16.8; *Gal3*$^{+/-}$, 81.9±7.6; *Gal3*$^{-/-}$, 74.4±7.6; df=11, F=0.42; P>0.5) (Fig. 3B,C). Although transit-amplifying progenitor cells are the major mitotic population in the SVZ, astrocytes and neuroblasts also divide. To exclude the possibility that loss of Gal-3 changed the ratio of SVZ proliferative cell types, we used triple immunohistochemistry (Fig. 3D–F). Proliferative astrocytes were labeled with BrdU and GFAP, proliferative neuroblasts with BrdU and Dcx, whereas BrdU$^+$ proliferative cells, which did not express GFAP or Dcx, were assumed to be mainly transit-amplifying progenitors (Fig. 3G) (Doetsch et al., 1997). The proportion of BrdU$^+$ GFAP$^+$ cells did not differ significantly between wild-type (9.18±2.61%), *Gal3*$^{+/-}$ (8.2±2.78%) and *Gal3*$^{-/-}$ (8.52±3.62%) littermates (df=11, F=0.108; P>0.5) (Fig. 3G). Similarly, no significant difference was observed in the percentage of BrdU$^+$ Dcx$^+$ cells (20.6±4.30% in wild-type littermates, 19.9±1.49% in *Gal3*$^{+/-}$ and 19.15±2.56% in *Gal3*$^{-/-}$; df=11, F=0.258; P>0.5). The percentage of BrdU$^+$ GFAP$^-$ Dcx$^-$ cells was also unchanged in *Gal3*-null mice.

Galectins cause increased cell death in many cell types (Yang et al., 1996). We first counted the number of Tunel$^+$ cells in the SVZ and found no differences between numbers in *Gal3*$^{-/-}$ and wild-type mice (Fig. 3H,I) (WT, 2.85±0.51; *Gal3*$^{+/-}$, 2.25±0.43; *Gal3*$^{-/-}$, 2.50±0.29; df=11, F=0.737; P>0.5). We next analyzed the expression of activated (cleaved) caspase-3, a protease that is expressed by cells undergoing apoptosis. We found no significant change in the number of caspase-3$^+$ cells in the SVZ (supplementary material Fig. S3A,B) (WT, 0.46±0.096; *Gal3*$^{+/-}$, 0.42±0.10; *Gal3*$^{-/-}$, 0.41±0.095, df=11, F=0.75; P>0.75).

Loss of Gal-3 reduces SVZ to OB migration in vivo

Gal-3 is known to affect cell adhesion (Zhao et al., 2010) and migration (Villa-Verde et al., 1995). To examine SVZ to OB migration, we injected BrdU over a period of 3 days and sacrificed mice 2 weeks after the last injection (Fig. 4A). Slowly dividing

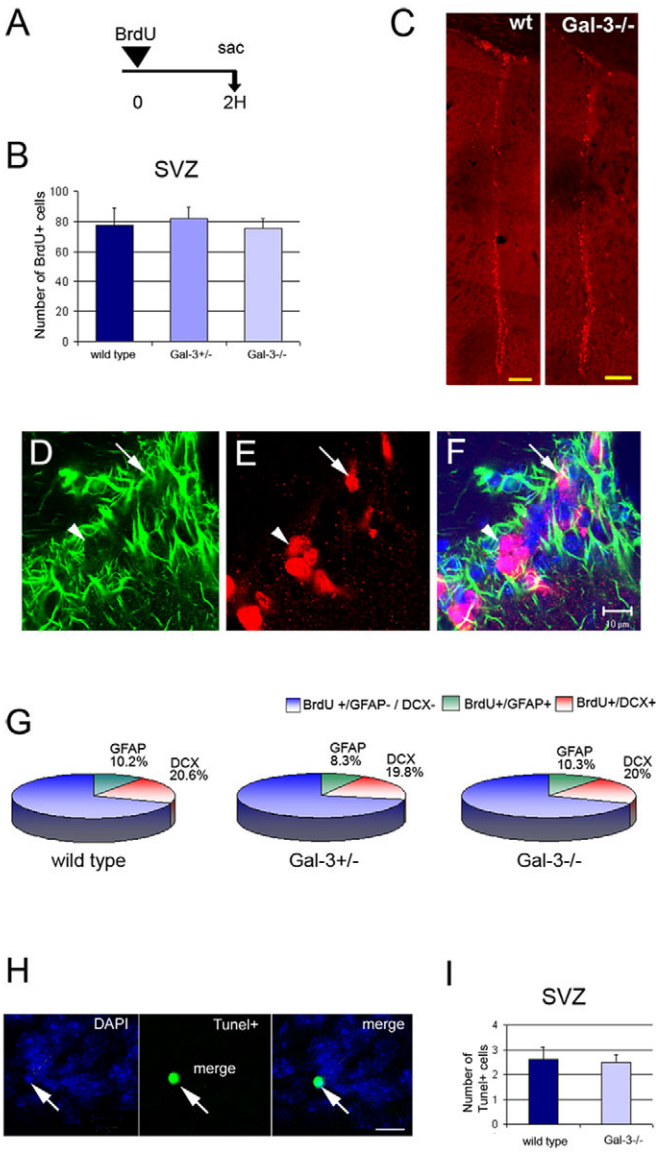

Fig. 3. Gal-3 does not affect SVZ proliferation or apoptosis. (**A**) Short-term BrdU regimen used to assess proliferation. (**B**,**C**) The number of BrdU$^+$ cells in the SVZ is not different in Gal-3 mutant mice compared with WT littermates. C shows a low magnification view of BrdU$^+$ cells in the lateral ventricle wall at a mid-striatal A–P level. Scale bars: 250 µm. (**D**–**F**) Confocal microscopy of GFAP immunofluorescence (D), BrdU (E), and merge with DAPI (F) from a *Gal3*$^{-/-}$ mouse. Arrow shows a BrdU$^+$ GFAP$^+$ cell and arrowhead, a BrdU$^+$ GFAP$^-$ cell. Scale bar: 10 µm. (**G**) The percentage of BrdU$^+$ cells that are GFAP$^+$ or Dcx$^+$ is not different in Gal-3 mutant mice. (**H**,**I**) The number of Tunel$^+$ cells in the SVZ is not altered in Gal-3 mutants. Scale bar: 5 µm. Error bars represent s.e.m.

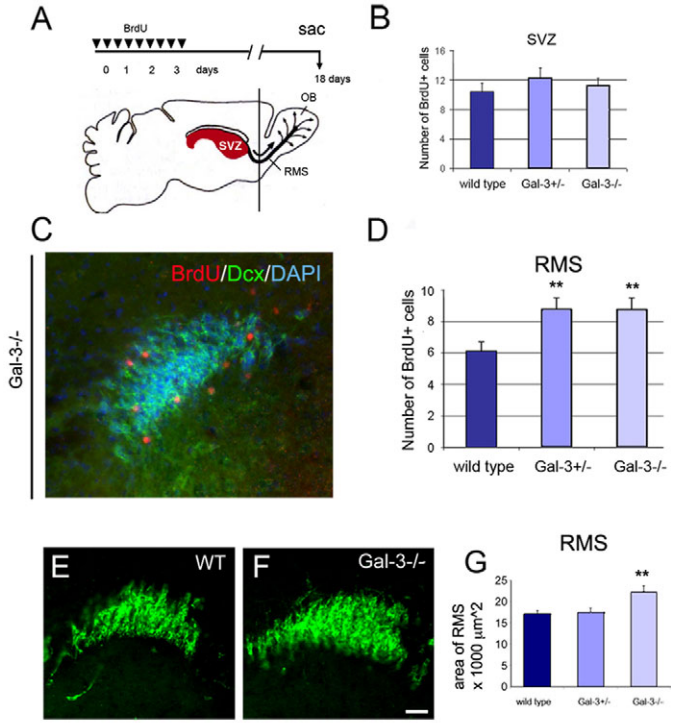

Fig. 4. Loss of Gal-3 increases the number of neuroblasts in the RMS. (**A**) Long-term BrdU regimen. (**B**) The number of BrdU$^+$ label-retaining cells in the SVZ is not significantly different in Gal-3 mutants. (**C**) Example of labeling for BrdU (red), Dcx (green) and DAPI (blue) in the RMS of a *Gal3*$^{-/-}$ mouse. (**D**) The number of BrdU$^+$ cells is increased in the RMS of mutants; $^{**}P<0.005$. (**E**,**F**) Dcx immunohistochemistry in the RMS of a WT and *Gal3*$^{-/-}$ mouse. Scale bar: 100 µm. (**G**) The surface area of the RMS, measured by outlining the perimeter of Dcx immunofluorescence, is increased in *Gal3*-nulls. $^{**}P<0.0001$. All error bars represent s.e.m.

SVZ stem cells can retain BrdU over long periods (Ferron et al., 2007). The number of BrdU-retaining cells in the SVZ was not altered (WT, 10.66±1.96; *Gal3*$^{+/-}$, 11.87±1.74; *Gal3*$^{-/-}$, 11.20±1.42, df=10, F=0.44; $P>0.5$) by loss of Gal-3 (Fig. 4B).

To assess neuroblast migration, we counted cells in the RMS and found significant increases in the number of BrdU$^+$ Dcx$^+$ cells in mutants compared with controls (WT, 1.96±0.26; *Gal3*$^{+/-}$, 3.0±0.5; *Gal3*$^{-/-}$, 2.8±0.24; df=11, F=8.76; $P<0.01$). The number of BrdU$^+$ cells was also significantly increased in the RMS of mutant compared with wild-type animals (Fig. 4C,D) (WT, 6.09±0.77; *Gal3*$^{+/-}$, 8.92±1.27; *Gal3*$^{-/-}$, 8.77±0.66; df=11, F=11.37; $P<0.005$). Confirming these data, the surface area of the RMS was significantly increased in *Gal3*$^{-/-}$ mice [WT, 16.59±0.3; *Gal3*$^{+/-}$, 15.14±1.2; *Gal3*$^{-/-}$, 20.35±1.3 (×1000) µm^2; df=11, F=26.35; $P<0.0001$] (Fig. 4E–G).

Two weeks after they are generated, most neuroblasts in the SVZ have reached the OB where they gradually lose Dcx and express neuronal nuclei (NeuN) as they differentiate (Fig. 5A–D) (Brown et al., 2003). The number of BrdU$^+$ NeuN$^+$ cells in the granular layer was significantly lower in *Gal3*$^{-/-}$ mice compared with wild-type littermates (Fig. 5E) [WT, 30.2±1.8; *Gal3*$^{+/-}$, 27.9±1.3; *Gal3*$^{-/-}$, 23.1±1.8 (×1000) mm^3; df=11, F=19.78; $P<0.001$]. This finding was corroborated by a significant overall loss of BrdU$^+$ cells in the granular layer of *Gal3*$^{-/-}$ mice (WT, 45±1.8; *Gal3*$^{+/-}$, 40.5±1.6; $P<0.01$; *Gal3*$^{-/-}$, 35±1.9; df=11, F=32.28; $P<0.0001$). Changes in the number of BrdU$^+$ NeuN$^+$ cells can be caused by altered rates of differentiation. However, the ratio of BrdU$^+$ NeuN$^+$ to the total number of BrdU$^+$ cells was not different between wild-type and mutant mice (WT, 67±1.6%; *Gal3*$^{+/-}$, 68.9±0.6%; *Gal3*$^{-/-}$, 65.8±2.3%; df=11, F=3.44; $P>0.5$). Qualitative analysis showed that BrdU$^+$ cells were evenly distributed in wild-type mice (data not shown), whereas the majority of BrdU$^+$ cells in the granular layer of *Gal3*$^{-/-}$ mice were located in deep layers (Fig. 5A–D), suggesting they had not yet migrated to superficial layers.

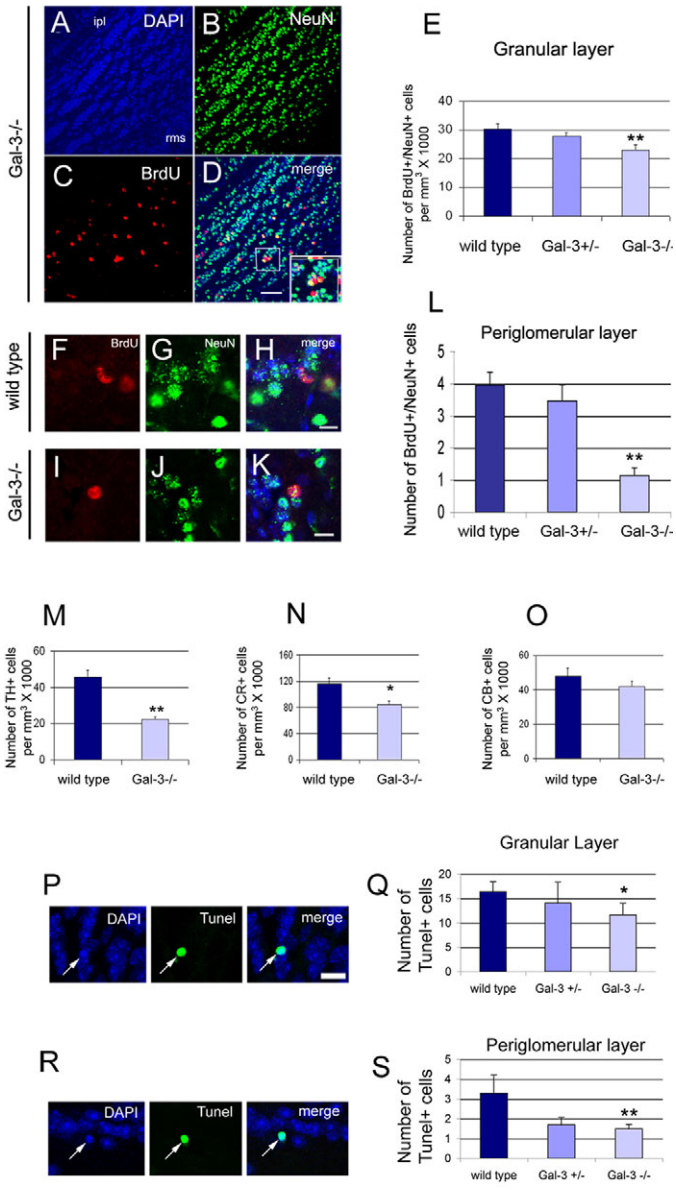

Fig. 5. *Gal3*-null mice have fewer new OB neurons. (**A**–**D**) Examples of BrdU and NeuN immunoreactivity in the OB granular layer of *Gal3*$^{-/-}$ mice. Note that most BrdU^{+} NeuN^{+} cells are in the deep granular layer near the RMS. (ipl, internal plexiform layer). Inset shows a double-labeled cell (yellow) at higher magnification. Scale bar: 50 μm. (**E**) The number of BrdU^{+} NeuN^{+} cells is significantly decreased in the granular layer of *Gal3*$^{-/-}$ mice. ***P*<0.001. (**F**–**H**) BrdU^{+} NeuN^{+} cells in the periglomerular layer of the OB of a WT mouse. Scale bar: 10 μm. (**I**–**K**) BrdU^{+} NeuN^{+} cells in the periglomerular layer of the OB of *Gal3*$^{-/-}$ mice. Scale bar: 10 μm. (**L**) The number of BrdU^{+} NeuN^{+} cells is significantly decreased in the periglomerular layer of *Gal3*$^{-/-}$ mice. ***P*<0.001. (**M**–**O**) The number of TH^{+} and CR^{+}, but not CB^{+}, cells decreases significantly in the OB of *Gal3*$^{-/-}$ mice. **P*<0.05, ***P*<0.005. (**P**,**Q**) The number of Tunel^{+} cells is significantly decreased in the OB granular layer. Arrows indicate a typical Tunel^{+} cell. Scale bar: 10 μm. **P*<0.05. (**R**,**S**) The number of Tunel^{+} cells is significantly decreased in the OB periglomerular layer. Arrows indicate a typical Tunel^{+} cell. Scale bar: 10 μm. ***P*<0.005. All error bars represent s.e.m.

We next determined whether Gal-3 affected the number of newly established neurons in the periglomerular layer. The number of BrdU^{+} cells in this layer was dramatically decreased in mutants (WT, 10.3±1.3; *Gal3*$^{+/-}$, 7.7±0.9; *Gal3*$^{-/-}$, 2.7±0.7; df=11, F=60.03; *P*<0.001). Similarly, the number of BrdU^{+} NeuN^{+} cells (Fig. 5F–L) decreased greatly in nulls compared with controls (WT, 4.0±0.4; *Gal3*$^{+/-}$, 3.5±0.5; *Gal3*$^{-/-}$, 1.1±0.2; df=11, F=54.56; *P*<0.001).

Tyrosine hydroxylase (TH^{+}), calretinin (CR^{+}), and calbindin (CB^{+}) interneurons in the periglomerular layer (supplementary material Fig. S4) are preferentially derived from SVZ subregions and sublineages (Merkle et al., 2007; Young et al., 2007). The number of TH^{+} and CR^{+} periglomerular interneurons was significantly decreased in mutants (Fig. 5M,N) [TH: WT, 45.8±3.6; *Gal3*$^{-/-}$, 22.0±1.5 (×1000) cells per mm^{3}, *P*<0.005; CR: WT, 116.4±8.7; *Gal3*$^{-/-}$, 84.5±4.6 (×1000) cells per mm^{3}, *P*<0.05], but the number of CB^{+} cells remained the same (Fig. 5O) [WT, 48.0±4.6; *Gal3*$^{-/-}$, 42.1±3.0 (×1000) cells per mm^{3}, *P*>0.1].

The decreased number of newborn neurons could be due to increased cell death; however, the number of Tunel^{+} cells also decreased in mutants in the granular layer (WT, 16.3±2.0; *Gal3*$^{+/-}$, 14.0±4.3; *Gal3*$^{-/-}$, 11.7±2.3; df=11, F=9.1; *P*<0.05) (Fig. 5P,Q) and the periglomerular layer (WT, 3.3±0.9; *Gal3*$^{+/-}$, 1.7±0.4; *Gal3*$^{-/-}$, 1.5±0.2; df=11, F=11.0; *P*<0.005) (Fig. 5R,S). Thus the decrease in OB neurons was not due to increased apoptosis, but was probably due to decreased migration.

Gal-3 modulates subcomponents of SVZ neuroblast migration

To confirm, and examine in more detail, the role of Gal-3 on neuroblast migration, we used two-photon time-lapse microscopy (Nam et al., 2007). SVZ cells were labeled with intraventricular injections of cell tracker green (CTG) (De Marchis et al., 2001) and migration was studied 2 days later (Fig. 6A–C) (supplementary material Movies 1 and 2). Using this strategy, we examined cells that had migrated long distances from the SVZ to the RMS. Wild-type neuroblasts migrated at an average speed of 106±7 μm/hour, which was similar to results of our previous studies (Kim et al., 2009; Nam et al., 2007). Neuroblasts moved significantly slower in mutants (*Gal3*$^{-/-}$, 84±3 μm/hour; *P*<0.05) (Fig. 6D), primarily as a result of decreased time spent in the fast phases of movement (WT, 13.6±2.8%; *Gal3*$^{-/-}$, 4.9±1%; *P*<0.05) (Fig. 6E). We next measured a parameter that is independent of speed, the migratory index (net distance over total distance). It was significantly decreased (WT, 0.61±0.01; *Gal3*$^{-/-}$, 0.48±0.03; *P*<0.01) (Fig. 6F), indicating that the *Gal3*$^{-/-}$ cells moved in a more complex local manner. Confirming this result, the net distance moved by neuroblasts in mutant mice decreased (Fig. 6G). These differences in motility subcomponents can be readily seen when the cell pathways are traced and shown in three dimensions (Fig. 6H,I). We also counted the percent cells exhibiting motility and showed there was no difference between groups of mice.

Secreted Gal-3 modulates migration from explants

The studies above could not distinguish whether secreted Gal-3 is sufficient to regulate neuroblast migration. To directly test this, we cultured RMS explants in the presence of either a blocking antibody specific for Gal-3 (clone M3/3828) (Inohara and Raz, 1995) or mouse recombinant rGal-3. We used postnatal day 4 mice because explant migration is more robust at this age (Ward and Rao, 2005) and we knew that Gal-3 is expressed in radial glia as well as astrocytes at this stage. The RMS was initially dissected from the OB core of Dcx–GFP mice (Fig. 7A), to confirm the identity of migrating cells. Only Dcx-GFP^{+} neuroblasts emigrated from the cultured explants (data not shown). Anti-Gal-3 blocking antibody

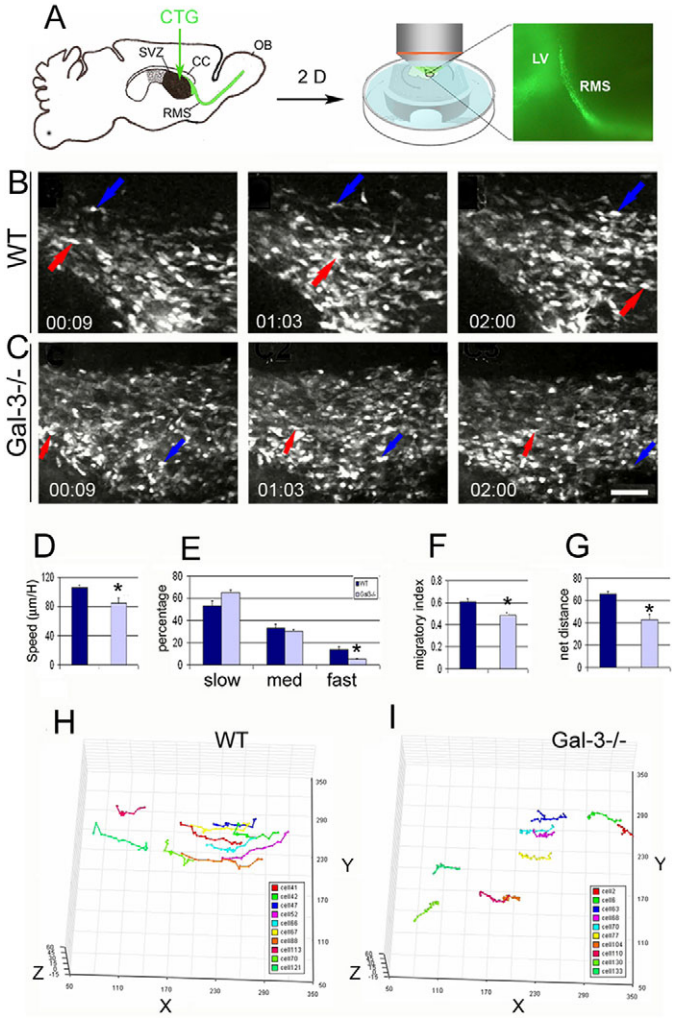

Fig. 6. Two-photon time-lapse microscopy reveals slower and more complex motility in *Gal3* null mice. (**A**) Cell tracker green was injected into the lateral ventricle and 2 days later neuroblast migration was analyzed at the RMS elbow in slices. Low-magnification photomicrograph on right shows CTG-labeled cells migrating in the RMS. (**B**) Still images from a two-photon time-lapse movie from a WT slice (supplementary material Movie 1). Colored arrows show the positions of two CTG-labeled neuroblasts. Time stamps are in hours:minutes. (**C**) Still images showing the positions of two CTG-labeled neuroblasts (colored arrows) in a *Gal3*$^{-/-}$ slice (supplementary material Movie 2). Scale bar: 50 µm. (**D**) Speed of migration is decreased in null mice compared with the WT. **P*<0.05. (**E**) The percentage of migrating cells in the fast migratory phase is significantly decreased in null mice compared with the WT. **P*<0.05. (**F**) The migratory index (net distance divided by total distance) is decreased in null mice compared with the WT. **P*<0.05. (**G**) The net distance of migrating neurons is decreased in null mice compared with the WT. **P*<0.01. (**H**,**I**) Tracks of individual neuroblast migration in WT and *Gal3*-null mice showing that null mouse neuroblasts exhibit decreased motility. Each color represents the path of a different cell. All error bars represent s.e.m.

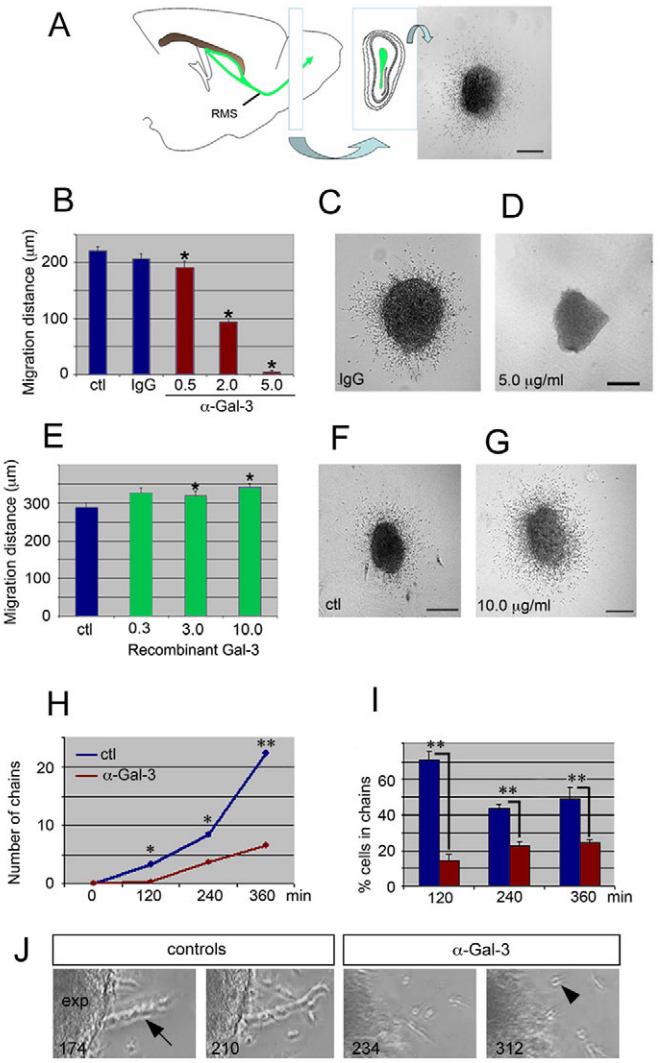

Fig. 7. Soluble Gal-3 increases SVZ neuroblast migration from explants. (**A**) Explants taken from the rostral part of the RMS of P4 Dcx–GFP mice and cultured in Matrigel for 48 hours show robust migration. (**B**) Gal-3 function-blocking antibody inhibits migration. Concentration of antibodies was in µg/ml. (**C**,**D**) Compared to IgG control, migration is blocked in 5.0 µg/ml anti-Gal-3. (**E**,**F**) Neuroblast migration increases in the presence of recombinant Gal-3. (**G–I**) The number of neuroblast chains and percentage of cells migrating in chains decreases after anti-Gal-3 treatment. (Error bars in H too small to be visible. All error bars represent s.e.m.) **P*<0.05, ***P*<0.005. Scale bars:100 µm. (**J**) Examples of chain migration (arrow) from control explants (exp) and individual cell migration (arrowhead) in anti-Gal-3 antibody treated explants. Frames taken from supplementary material Movie 3, time-stamps indicate minutes after plating of explant.

inhibited neuroblast migration after 48 hours in a dose-dependent manner, whereas control IgG had no effect on the average distance migrated (Ctl, 222±5; Ctl IgG, 212±14; 0.5 µg/ml Gal-3 antibody, 193±9; 2.0 µg/ml, 98±5; 5.0 µg/ml, 7±1; df=59, F=1.553; *P*<0.0005) (Fig. 7B–D). These results were confirmed with time-lapse microscopy (supplementary material Movie 3). Indeed, migration from explants was delayed and severely reduced in the presence of 2.0 µg/ml of anti-Gal-3 after 4 hours (supplementary material Movie 3). In contrast to the function blocking antibody, rGal-3 significantly increased migration in a dose-dependent fashion (Fig. 7E–G) (Ctl, 282±11; 0.3 µg/ml rGal-3, 337±12; 3 µg/ml, 327±8; 10 µg/ml, 345±7; df=47, F=229.7; *P*<0.001).

We next examined whether anti-Gal-3 antibodies affected chain migration. Both the number of neuroblast chains (Fig. 7H–J), as well as the percentage of cells migrating in chains (Fig. 7I), was

significantly reduced with 2 μg/ml of anti-Gal-3. The number of chains was maximally decreased 6 hours after treatment (22.3±1.2 versus 6.7±0.3, $P<0.05$). At 6 hours, the percentage of cells in chains was decreased from 48.8±6.6% in controls to 24.5±2.0% ($P<0.05$). These observations suggest that secreted Gal-3 modulates various aspects of neuroblast migration in vitro.

Reduced expression of phosphorylated EGFR in *Gal3*$^{-/-}$ mice

Gal-3 physically interacts with the EGFR (Partridge et al., 2004) and activation of EGFR decreases neuronal migration (Kim et al., 2009). To test whether Gal-3 regulates EFGR expression, we performed western blots using an antibody specific for EGFR ($n=3$ experiments). No difference in EGFR expression was observed in *Gal3*$^{-/-}$ mice compared with wild-type SVZs (Fig. 8A,B). EGFR phosphorylation is necessary for its activation; interestingly, phosphorylated EGFR was significantly increased in *Gal3*$^{-/-}$ compared with wild-type SVZs (Fig. 8A,B) ($P<0.05$) ($n=3$ experiments). These results suggest that Gal-3 either directly or indirectly inhibits EGFR phosphorylation. However, co-immunoprecipitation assays ($n=3$ experiments) revealed that in the SVZ, Gal-3 does not bind to EGFR (data not shown).

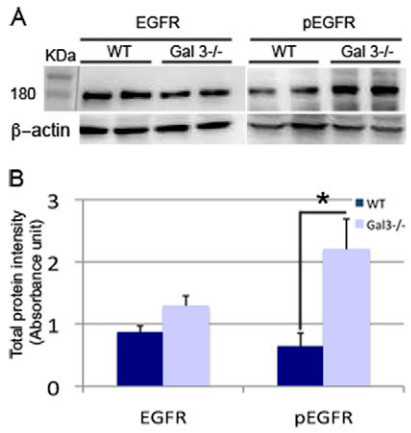

Fig. 8. Phosphorylated EGFR expression is increased in the SVZ of *Gal3*$^{-/-}$ mice. (**A**,**B**) Western blots and quantification show that basal levels of EGFR are unchanged in mutant mice. By contrast, phosphorylated EGFR is significantly upregulated in *Gal3*$^{-/-}$ mice.

Discussion

Although the function of Gal-3 has been extensively studied in the regulation of inflammation and cancer, its role in the normal brain was unknown. This study shows that Gal-3 is constitutively expressed in the adult SVZ and along the normal route of neuroblast migration. In addition, we provide evidence that secreted Gal-3, by maintaining the niche cytoarchitecture, modulates neuroblast migratory behavior without affecting SVZ proliferation or apoptosis. Although Gal-3 is known to influence migration in other cell types, to our knowledge this is the first evidence that it modulates neuronal migration.

Galectin-3 maintains SVZ and RMS cytoarchitecture

It was previously known that in the context of brain injury and other pathological conditions, Gal-3 becomes expressed by activated microglia. However, its expression in normal brain had never been reported. In this study, immunohistochemistry showed selective Gal-3 expression in the SVZ and RMS, which are areas that exhibit the most extensive neurogenesis and migration in adult brains. These results are supported by the localization of *Gal3* transcripts in the SVZ and RMS (Ng et al., 2009). We hypothesized that microglia, which are constitutively semi-activated in the SVZ, are the cells that express Gal-3 in this region. However, SVZ microglia were only weakly associated with Gal-3 expression, suggesting that neural rather than hematopoietic cells express it.

Indeed, Gal-3 immunoreactivity was associated with astrocyte and ependymal cells. Because ependymal cells and astrocytes lining the lateral ventricles arise from radial glia (Spassky et al., 2005; Tramontin et al., 2003), it was not surprising that postnatal SVZ radial glia also expressed Gal-3. Our EM studies showed that both astrocyte and ependymal cell cytoplasm contained Gal-3 immunoprecipitates. A subset of astrocyte nuclei also contained Gal-3 immunoprecipitates. Nuclear Gal-3 participates in splicing of pre-mRNA (Haudek et al., 2010), and it is tempting to speculate that its differential cell compartment expression in the SVZ might underlie some of the differences between SVZ astrocytes and ependymal cells. A recent study using human GFAP–GFP and prominin labeling to isolate SVZ stem cells shows they exhibit high levels of Gal-3 (Beckervordersandforth et al., 2010). Future FACsorting approaches might confirm SVZ cell subtype expression of Gal-3 (Pastrana et al., 2009). Interestingly, although Gal-3 expression lined the migratory route, both light and electron microscopy showed that it was not expressed by neuroblasts themselves. Our current data support the notion that Gal-3 is expressed in the SVZ and RMS by SVZ astrocytes and ependymal cells, but is lost in most of their progeny. These observations suggest that Gal-3 is well positioned to regulate the SVZ niche.

Because Gal-3 was expressed by both astrocytes and ependymal cells, it was not altogether surprising to find that loss of Gal-3 resulted in abnormal astrocytic and ependymal cytoarchitecture in the SVZ. Astrocytes had thickened GFAP immunoreactivity within their processes and distorted morphology throughout the SVZ and RMS. GFAP is an intermediate filament cytoskeletal protein and antibodies against it do not reveal astrocyte plasma membranes. Although we do not believe it is likely, it is possible that widths of GFAP immunoreactivity increased without the entire process thickening. Gal-3 promotes process outgrowth in dorsal root ganglion neurons (Pesheva et al., 1998) and axonal branching in hippocampal neurons (Diez-Revuelta et al., 2010), suggesting that it regulates morphology in a variety of neural cells. Disrupted SVZ and RMS astrocytic cytoarchitecture has been associated with abnormal migration in *Bax*-null mice (Kim et al., 2007) and ErbB4 mutants (Ghashghaei et al., 2006).

Another cellular mechanism that might influence SVZ neuroblast migration is the beating of ependymal cell cilia, which establishes gradients of chemorepellents in the SVZ (Sawamoto et al., 2006). We found a marked decrease in the density of ependymal cilia, suggesting that CSF flow is disrupted in *Gal3*-null mice. These results suggests that Gal-3 might have a role in forming and maintaining SVZ niche cytoarchitecture and influences neuroblast migration by a combination of maintaining astrocyte glial tubes and ciliary integrity.

Gal-3 maintains normal SVZ neuroblast migration

Gal-3 is known to influence proliferation of endometrial cells (Lei et al., 2009) and preadipocytes (Kiwaki et al., 2007) by inhibiting and stimulating cell division, respectively. Gal-1 is also expressed by SVZ astrocytes and promotes cell proliferation (Sakaguchi et

al., 2006). Thus, we hypothesized that Gal-3 influences cell proliferation in the adult SVZ; however, basal rates of proliferation were unchanged. SVZ stem cells self-renew with infrequent mitoses, and similarly to more rapidly dividing cells, there was no change in the number of label-retaining cells. Thus Gal-3 does not seem to affect multiple types of cell proliferation in the adult SVZ.

Apart from its proliferative role, Gal-3 is also known to act as an adhesion and de-adhesion molecule (Friedrichs et al., 2008) and its pattern of expression in the SVZ led us to study neuroblast migration. Furthermore, Gal-3 binds β-galactoside residues on EGFR, laminin, β1 integrin, NCAM and tenascin, all of which influence SVZ neuroblast migration (Aguirre et al., 2005; Cremer et al., 1994; Emsley and Hagg, 2003; Ghashghaei et al., 2007; Kim et al., 2009). We found significantly fewer newborn neurons in the periglomerular and granule layers of the OB in *Gal3*-null mice 2 weeks after BrdU administration, suggesting decreased migration. In addition, the RMS size and number of newborn neurons in the RMS of *Gal3*-null mice was increased 2 weeks after BrdU injection. This might reflect cell accumulation due to inefficient migration. The greater RMS size might also have been partially caused by increased thickness of $GFAP^+$ astrocytic processes. Although SVZ apoptosis did not seem to change in the *Gal3*-null mice, decreased numbers of $Tunel^+$ cells in the OB of these mice were observed and could be explained by lower rates of neurons reaching the OB and then undergoing apoptosis. Taken together, the in vivo data suggest that in the absence of Gal-3, SVZ cell migration is disrupted.

Although our in vivo studies strongly suggested that Gal-3 maintains migration, lack of Gal-3 did not completely stop migration because the OB size in mutant was unchanged. We used two-photon time-lapse microscopy to image migration at a finer spatiotemporal scale and dissect which aspects of migration might have been affected by Gal-3. We chose the RMS because all SVZ cells funnel through it before reaching the OB and because in vivo evidence suggested decreased RMS migration in *Gal3*-null animals. Two-photon time-lapse imaging previously revealed that only a subset of neuroblasts are migratory at any time and that they migrate in multiple directions, at different speeds and in long distance rostral and local exploratory patterns (Nam et al., 2007). Importantly, CTG-labeled neuroblasts in wild-type mice in this study moved at very similar speeds to migratory $GAD–GFP^+$ cells in our previous study (Nam et al., 2007), suggesting that CTG did not alter migration. Neuroblasts in *Gal3*-null mice migrated more slowly and exhibited more exploratory motility. They moved shorter net distances, corroborating the increases in exploratory motility. These direct observations provide compelling evidence that Gal-3 maintains speed and straightness of migration, two parameters that synergize efficient rostral migration. Taken together, we interpret our data to suggest that decreasing these specific components of migration is sufficient to significantly delay migration and thereby decrease rates of OB neurogenesis.

Secreted Gal-3 promotes neuroblast migration

Gal-3 has cell-autonomous effects, as well as cell surface and secreted paracrine effects (Ochieng et al., 2004). Therefore we used acute in vitro RMS explants from wild-type mice to examine the role of secreted Gal-3 in migration. Previously validated anti-Gal-3 functional blocking antibodies (Fukushi et al., 2004) decreased neuroblast migration dose-dependently, whereas control IgG antibodies did not. It is possible that the anti-Gal-3 antibodies decreased migration through a simple steric hindrance mechanism rather than by decreasing Gal-3 function. However, our function-blocking antibody studies matched the decreased migration in $Gal3^{-/-}$ slices and in vivo, and the control IgG antibody had no effect on migration. In contrast to anti-Gal-3, recombinant Gal-3 increased migration distances. Thus, these studies confirmed that Gal-3 directly and acutely affects SVZ migration, adding credence to our in vivo and slice data from the mutant mice.

We also showed that loss of Gal-3 function decreases chain formation in vitro; the number of chains and the percentage of cells migrating in chains decreased dramatically in response to the blocking antibody. In addition, our in vivo analysis suggested that the number of neuroblasts migrating individually was increased in $Gal3^{-/-}$ mice. Thus, secreted Gal-3 might contribute to chain formation and maintenance.

Gal-3 might affect migration via the EGFR

Epidermal growth factor drives proliferation in the SVZ (Kuhn et al., 1997; Reynolds and Weiss, 1992) and helps maintain its balance of stem and progenitor cells (Doetsch et al., 2002). We recently showed that a subset of SVZ neuroblasts retains EGFR expression, $EGFR^+$ neuroblasts moved more slowly and in a more exploratory manner, and when EGFR was stimulated, the percentage of migrating neuroblasts decreased (Kim et al., 2009). Thus it seems that EGFR signalling also mediates major transitions in the SVZ by pushing cells backwards to a non-migratory phenotype. We show in this study that, similar to $EGFR^+$ neuroblasts, loss of Gal-3 decreased speed and increased migration complexity. This was accompanied by increases in phosphorylated EGFR (active form) in $Gal3^{-/-}$ mice. Such an interaction has been recently described in pancreatic cancer cells: knockdown of Gal-3 increases phosphorylated EGFR (Merlin et al., 2011). Gal-3 interacts with glycoproteins such as the EGFR (Partridge et al., 2004) and the neuronal adhesion molecule L1 (Diez-Revuelta et al., 2010), proteins that regulate neuronal migration. Gal-3 is thought to crosslink EGFR, stabilize them and reduce endocytosis (Partridge et al., 2004). In this study, using co-immunoprecipitation we did not detect physical binding between Gal-3 and EGFR. Overall, our results suggest that loss of Gal-3 decreases SVZ neuroblast migration by indirectly increasing EGFR activation in neuroblasts.

Conclusion

Galectins have important actions in pathological inflammation (Sato and Nieminen, 2004) and cancer, but their potential function in normal neurodevelopmental processes has been under-explored. In this study, we show that Gal-3 is necessary for normal SVZ migration. Carbohydrates are essential for neural development, and glycoconjugates seem to be particularly important in the modulation of SVZ migration (Ono et al., 1994). This study expands our understanding of the promigratory niche by introducing a sugar-binding molecule as a modulator of important neuroblast migration parameters and might lead to the development of new strategies designed to allow neuroblast migration to human brain damage.

Materials and Methods

Animal use

P4 and adult (6–8 week) CD1 mice were obtained from Charles River Laboratories (Margate, UK), adult wild-type, $Gal3^{+/-}$ and $Gal3^{-/-}$ littermates on 129Sv background from Francoise Poirier (Colnot et al., 1998). Doublecortin–GFP mice were generated at the Gensat BAC project at Rockefeller University. All procedures were carried out with Oxford University Research Ethics Committee approval, in accordance with the Animals (Scientific Procedures) Act of 1986 (UK). All efforts were made to minimize animal suffering and distress.

Bromodeoxyuridine injections

To examine proliferation, a cohort of mice received one injection of 50 mg/kg bromodeoxyuridine (BrdU) (Sigma) i.p., 2 hours before perfusion and sacrifice (n=4 for WT, *Gal3*$^{+/-}$, *Gal3*$^{-/-}$). To examine migration, another cohort received three injections of BrdU (50 mg/kg, i.p.) per day for 3 days and were sacrificed 2 weeks after the last injection (n=4 for WT, *Gal3*$^{+/-}$, *Gal3*$^{-/-}$).

Immunohistochemistry

Immunohistochemical detection of BrdU and proteins was carried as described previously (Kim et al., 2010). We used the following primary antibodies: mouse anti-acetylated tubulin (1:1000; Sigma), rabbit anti-β-catenin (1:1000; Sigma), goat anti-CD45 (1:500; Santa Cruz Biotechnology, Santa Cruz, USA), mouse anti-Mash1 (1:500; Pharmingen), rabbit anti-Gal-3 (1:100; Santa Cruz Biotechnology), goat anti-GFAP (1:500; Santa Cruz Biotechnology), mouse anti-PSA-NCAM (1:500; Chemicon, Temecula, CA), mouse anti-NeuN (1:500; Chemicon), goat anti-vimentin (1:100; Santa Cruz Biotechnology), rabbit anti-tyrosine hydroxylase (1:2000; Chemicon), rabbit anti-calretinin (1:2000; Chemicon) and rabbit anti-calbindin (1:500; Chemicon). The secondary antibodies used were conjugated to Streptavidin Alexa Fluor 546 (1:500, Invitrogen, Paisley, UK), Alexa Fluor 488 (1:500; Invitrogen) or Cy3 (1:500; Jackson ImmunoResearch). We routinely checked for aberrant background staining of secondary antibodies by omitting the primary antibodies.

All BrdU-positive cells along the wall of the lateral ventricle and RMS were counted in at least ten evenly spaced sections per animal, from coordinates –0.40 to 1.33 relative to Bregma using a 40× lens. BrdU$^+$ NeuN$^+$ TH$^+$ CB$^+$ CR$^+$, cells were counted in at least ten evenly spaced sections of olfactory bulb per animal at 40× using confocal microscopy, in five optical sections separated by 2 µm each. The total number of cells per mm^3 was calculated. The total number of BrdU$^+$ TH$^+$, BrdU$^+$ CB$^+$ and BrdU$^+$ CR$^+$ cells present in the entire periglomerular layer of ten evenly spaced olfactory bulb sections per animal was counting using a confocal microscope. Investigators were blind to the genotype for all quantifications.

TUNEL labeling

Sections were rinsed twice in Tris-buffered saline (TBS), dehydrated and rehydrated in graded isopropanol, rinsed twice in TBS, and pre-incubated with terminal transferase (TdT) buffer (Roche) for 15 minutes at 37°C. Positive control sections were treated with 2 mg/ml DNase (Sigma) for 15 minutes. Subsequently, sections were incubated in TdT mixture (Roche) for 30 minutes at 37°C, rinsed three times in TBS. Six evenly spaced sections per animal were analyzed from Bregma +1.2 to –0.5 in the SVZ and Bregma +3.8 to +5.8 in the OB (n=4 WT, n=4 *Gal3*$^{-/-}$). The total number of positive cells per section in the SVZ, OB periglomerular and granular layer, was counted with the investigator blind to genotype.

Whole mounts

Dissection of the lateral wall and immunostaining were performed as previously described (Mirzadeh et al., 2008) on n=3 WT and n=3 *Gal3*$^{-/-}$ mice.

Immunoelectron microscopy

The experiment was performed as previously described (Moss and Bolam, 2008) on n=3 WT and n=3 *Gal3*$^{-/-}$ mice.

Image acquisition

Epifluorescent microscopy images were obtained on a Leica DMIRB with a digital camera (Hamamatsu C4742-95) and analyzed with Openlab 5. Colocalization studies were carried out using confocal microscopy (Zeiss LSM 710). Optical sections (Z=0.5 µm) were sequentially acquired using a 63× oil objective lens and Zeiss LSM image 5 software used to merge images.

Two-photon time-lapse microscopy

10 mM cell tracker green (CTG) (CMFDA, Molecular Probes) in DMSO was injected into lateral ventricle as previously described (Kim et al., 2009) (stereotactic coordinates A-P 0.1, M-L 0.70, D–V 2.5 from bregma for WT; A–P 0.15, M–L 0.70, D–V 2.5 for *Gal3*$^{-/-}$). Migration was imaged 2 days later. Brains were submerged in ice-cold artificial cerebrospinal fluid (aCSF; 125 mM NaCl, 2.5 mM KCl, 2 mM, $CaCl_2$, 1 mM $MgCl_2$, 26 mM $NaHCO_3$, 1.25 mM H_2PO_4, and 25 mM glucose at pH 7.4) and 300 µm sagittal slices cut on a Vibratome (Campden Instruments). Brain slices were treated as previously described (Nam et al., 2007). A custom-built two-photon imaging system (Nam et al., 2007) was used to acquire a stack of 51 optical sections (separated by 1 µm) every 3 minutes. Oxygenated aCSF was continuously perfused throughout imaging at 0.5–1.0 ml/minute.

Two-photon time-lapse analysis

Two-photon images were acquired by Fluoview software (Olympus) and imported into Volocity software (Improvision) for processing and quantification. Collapsed stacks of 3D images were exported into Quicktime (Apple) to generate 2D time-lapse movies. For quantifying percentage of motile cells, cells that moved over two cell diameters were numbered and traced over the first 1 hour. Then, 3D coordinates of cells were recorded over the first 1 hour period. Only cells that were traceable for the entire hour were included in speed and migratory index analysis. A random number generator randomly selected ten such cells. Any slice drifting was adjusted by aligning stationary cells across frames. Total distance was defined as the sum of all frame-to-frame cell movements from a given cell's trajectory, and net distance was defined as the distance between the initial and final cell positions. Migratory index was defined as the net distance divided by total distance. If the migratory index was less than 0.4, between 0.4 and 0.6, or more than 0.6, cells were classified as exploratory, intermediate, or migratory, respectively. For speed analysis, if cells moved from frame to frame less than 100 µm/hour, between 100 and 200 µm/hour, or more than 200 µm/hour, each movement was categorized as slow, intermediate, and fast respectively.

Explant culture and time-lapse microscopy

Explants were prepared as previously described (Ward and Rao, 2005). These explants were embedded in 33% Matrigel (BD Biosciences, San Jose, CA) supplemented with 2.5 mg/ml collagen type I (BD Biosciences) and kept for 48 hours at 37°C and 5% CO_2. Explants were cultured in DMEM with 10% fetal bovine serum, penicillin-streptomycin, with anti-mouse Gal-3 function-blocking rat monoclonal antibody (clone M3/38; Santa Cruz Biotechnology) or control rat IgG (Santa Cruz Biotechnology). Alternatively, explants were incubated with mouse recombinant Gal-3 (R&D systems, Minneapolis, MN) or equivalent volumes of solvent (PBS+ 0.1% BSA). For time-lapse, explants were cultured in humidified chambers at 37°C and aerated with 5% CO_2. Pictures were taken every 6 minutes using a digital camera (Hamamatsu C4742-95, Shizouka, Japan) and a Leica DMIRB inverted microscope and analyzed with Openlab 5 software (Improvision, Coventry, UK). Cell migration was first analyzed in explants from Dcx–GFP mice to confirm the neuroblast identity of migrating cells (n=20 explants). Quantification of cell migration was then performed on explants from CD-1 mice (at least 50 explants for each condition). Migration distances were measured on 10× digitized images as the distance between the edge of the explant and the farthest cells. Eight measurements per explant were performed covering the totality of the area of migration using Openlab 5. To study chain migration from the explants, image frames were analyzed at 120, 240 and 360 minutes. 'Chains' were defined as clusters of at least three contiguous cells. The percentage of cells emigrating in chains was determined as the ratio of cells in chains over the total number of cells having emigrated from the explant (n=3 explants for each condition).

Western blot and densitometric analysis

SVZ tissue from WT and *Gal3*$^{-/-}$ mice were homogenized in lysis buffer (0.025M Tris-HCl, 0.15 M NaCl, 0.001 M EDTA, 1% NP-40, 5% glycerol; pH 7.4). Proteins were separated by SDS-PAGE under reducing conditions and transferred to nitrocellulose membranes. Membranes were blocked with 5% skimmed milk in TBS at room temperature for 1 hour. Membranes were then incubated with either anti-EGFR (1:500; Sigma), anti-pEGFR Tyr1173 (1:1000; Millipore) or anti-beta-actin (1:200; Sigma) overnight at 4°C. Membranes were next incubated with HRP-conjugated secondary IgGs (1:500) for 1 hour. All membranes were visualized using luminol reagent (Bio-Rad). Densitometric analysis of the membrane was performed using a Model imaging densitometer (Bio-Rad) in transmittance mode and analyzed using ImageJ software.

Statistics

Data are presented as mean ± s.e.m. Differences between two different groups were assessed using two-tailed Student's t-test and differences amongst three or more groups with one-way ANOVA. Groups were considered significantly different when at least a 95% confidence level (P<0.05) was obtained.

We would like to thank Tien Dang for technical assistance, Delphine Delacour for critical reading of the manuscript, and Yi Rao's laboratory for help with the explant method. We thank members of the Szele lab for critical reading of the manuscript. F.G.S. was supported by NIH grant NS-42253, C.C.Y. by a Rhodes scholarship and F.P. by Association contre le Cancer (grant #1113). Deposited in PMC for release after 12 months.

Supplementary material available online at
http://jcs.biologists.org/cgi/content/full/124/14/2438/DC1

References

Aguirre, A., Rizvi, T. A., Ratner, N. and Gallo, V. (2005). Overexpression of the epidermal growth factor receptor confers migratory properties to nonmigratory postnatal neural progenitors. *J. Neurosci.* **25**, 11092-11106.

Barondes, S. H., Castronovo, V., Cooper, D. N., Cummings, R. D., Drickamer, K., Feizi, T., Gitt, M. A., Hirabayashi, J., Hughes, C., Kasai, K. et al. (1994). Galectins: a family of animal beta-galactoside-binding lectins. *Cell* **76**, 597-598.

Beckervordersandforth, R., Tripathi, P., Ninkovic, J., Bayam, E., Lepier, A., Stempfhuber, B., Kirchhoff, F., Hirrlinger, J., Haslinger, A., Lie, D. C. et al. (2010). In vivo fate mapping and expression analysis reveals molecular hallmarks of prospectively isolated adult neural stem cells. *Cell Stem Cell* **7**, 744-758.

Brown, J. P., Couillard-Despres, S., Cooper-Kuhn, C. M., Winkler, J., Aigner, L. and Kuhn, H. G. (2003). Transient expression of doublecortin during adult neurogenesis. *J. Comp. Neurol.* **467**, 1-10.

Colnot, C., Fowlis, D., Ripoche, M. A., Bouchaert, I. and Poirier, F. (1998). Embryonic implantation in galectin 1/galectin 3 double mutant mice. *Dev. Dyn.* **211**, 306-313.
Cremer, H., Lange, R., Christoph, A., Plomann, M., Vopper, G., Roes, J. R., Brown, R., Baldwin, S., Kraemer, P., Scheff, S. et al. (1994). Inactivation of the N-CAM gene in mice results in size reduction of the olfactory bulb and deficits in spatial learning. *Nature* **367**, 455-459.
De Marchis, S., Fasolo, A., Shipley, M. and Puche, A. (2001). Unique neuronal tracers show migration and differentiation of SVZ progenitors in organotypic slices. *J. Neurobiol.* **49**, 326-338.
Delacour, D., Koch, A. and Jacob, R. (2009). The role of galectins in protein trafficking. *Traffic* **10**, 1405-1413.
Diez-Revuelta, N., Velasco, S., Andre, S., Kaltner, H., Kubler, D., Gabius, H. J. and Abad-Rodriguez, J. (2010). Phosphorylation of adhesion- and growth-regulatory human galectin-3 leads to the induction of axonal branching by local membrane L1 and ERM redistribution. *J. Cell Sci.* **123**, 671-681.
Doetsch, F., Garcia-Verdugo, J. M. and Alvarez-Buylla, A. (1997). Cellular composition and three-dimensional organization of the subventricular germinal zone in the adult mammalian brain. *J. Neurosci.* **17**, 5046-5061.
Doetsch, F., Petreanu, L., Caille, I., Garcia-Verdugo, J. M. and Alvarez-Buylla, A. (2002). EGF converts transit-amplifying neurogenic precursors in the adult brain into multipotent stem cells. *Neuron* **36**, 1021-1034.
Elola, M. T., Wolfenstein-Todel, C., Troncoso, M. F., Vasta, G. R. and Rabinovich, G. A. (2007). Galectins: matricellular glycan-binding proteins linking cell adhesion, migration, and survival. *Cell. Mol. Life Sci.* **64**, 1679-1700.
Emsley, J. G. and Hagg, T. (2003). alpha6beta1 integrin directs migration of neuronal precursors in adult mouse forebrain. *Exp. Neurol.* **183**, 273-285.
Ferron, S. R., Andreu-Agullo, C., Mira, H., Sanchez, P., Marques-Torrejon, M. A. and Farinas, I. (2007). A combined ex/in vivo assay to detect effects of exogenously added factors in neural stem cells. *Nat. Protoc.* **2**, 849-859.
Friedrichs, J., Manninen, A., Muller, D. J. and Helenius, J. (2008). Galectin-3 regulates integrin alpha 2beta 1-mediated adhesion to collagen-I and -IV. *J. Biol. Chem.* **28**, 32264-32272.
Fukushi, J., Makagiansar, I. T. and Stallcup, W. B. (2004). NG2 proteoglycan promotes endothelial cell motility and angiogenesis via engagement of galectin-3 and alpha3beta1 integrin. *Mol. Biol. Cell* **15**, 3580-3590.
Ghashghaei, H. T., Weber, J., Pevny, L., Schmid, R., Schwab, M. H., Lloyd, K. C., Eisenstat, D. D., Lai, C. and Anton, E. S. (2006). The role of neuregulin-ErbB4 interactions on the proliferation and organization of cells in the subventricular zone. *Proc. Natl. Acad. Sci. USA* **103**, 1930-1935.
Ghashghaei, H. T., Lai, C. and Anton, E. S. (2007). Neuronal migration in the adult brain: are we there yet? *Nat. Rev. Neurosci.* **8**, 141-151.
Goings, G. E., Kozlowski, D. A. and Szele, F. G. (2006). Differential activation of microglia in neurogenic versus non-neurogenic regions of the forebrain. *Glia* **54**, 329-342.
Haudek, K. C., Spronk, K. J., Voss, P. G., Patterson, R. J., Wang, J. L. and Arnoys, E. J. (2010). Dynamics of galectin-3 in the nucleus and cytoplasm. *Biochim. Biophys. Acta* **1800**, 181-189.
Hirabayashi, J. and Kasai, K. (1993). The family of metazoan metal-independent beta-galactoside-binding lectins: structure, function and molecular evolution. *Glycobiology* **3**, 297-304.
Inohara, H. and Raz, A. (1995). Functional evidence that cell surface galectin-3 mediates homotypic cell adhesion. *Cancer Res.* **55**, 3267-3271.
Ishibashi, S., Kuroiwa, T., Sakaguchi, M., Sun, L., Kadoya, T., Okano, H. and Mizusawa, H. (2007). Galectin-1 regulates neurogenesis in the subventricular zone and promotes functional recovery after stroke. *Exp. Neurol.* **207**, 302-313.
Kariya, Y. and Gu, J. (2009). Roles of laminin-332 and alpha6beta4 integrin in tumor progression. *Mini Rev. Med. Chem.* **9**, 1284-1291.
Kim, W. R., Kim, Y., Eun, B., Park, O. H., Kim, H., Kim, K., Park, C. H., Vinsant, S., Oppenheim, R. W. and Sun, W. (2007). Impaired migration in the rostral migratory stream but spared olfactory function after the elimination of programmed cell death in Bax knock-out mice. *J. Neurosci.* **27**, 14392-14403.
Kim, Y., Comte, I., Szabo, G., Hockberger, P. and Szele, F. G. (2009). Adult mouse subventricular zone stem and progenitor cells are sessile and epidermal growth factor receptor negatively regulates neuroblast migration. *PLoS ONE* **4**, e8122.
Kim, Y., Wang, W. Z., Comte, I., Pastrana, E., Tran, P. B., Brown, J., Miller, R. J., Doetsch, F., Molnar, Z. and Szele, F. G. (2010). Dopamine stimulation of postnatal murine subventricular zone neurogenesis via the D3 receptor. *J. Neurochem.* **114**, 750-760.
Kiwaki, K., Novak, C. M., Hsu, D. K., Liu, F. T. and Levine, J. A. (2007). Galectin-3 stimulates preadipocyte proliferation and is up-regulated in growing adipose tissue. *Obesity (Silver Spring)* **15**, 32-39.
Kuhn, H. G., Winkler, J., Kempermann, G., Thal, L. J. and Gage, F. H. (1997). Epidermal growth factor and fibroblast growth factor-2 have different effects on neural progenitors in the adult rat brain. *J. Neurosci.* **17**, 5820-5829.
Kuwabara, I. and Liu, F. T. (1996). Galectin-3 promotes adhesion of human neutrophils to laminin. *J. Immunol.* **156**, 3939-3944.
Lei, C. X., Zhang, W., Zhou, J. P. and Liu, Y. K. (2009). Interactions between galectin-3 and integrinbeta3 in regulating endometrial cell proliferation and adhesion. *Hum. Reprod.* **24**, 2879-2889.
Liu, F. T., Patterson, R. J. and Wang, J. L. (2002). Intracellular functions of galectins. *Biochim. Biophys. Acta* **1572**, 263-273.
Luskin, M. B. (1993). Restricted proliferation and migration of postnatally generated neurons derived from the forebrain subventricular zone. *Neuron* **11**, 173-189.
Merkle, F. T., Mirzadeh, Z. and Alvarez-Buylla, A. (2007). Mosaic organization of neural stem cells in the adult brain. *Science* **317**, 381-384.
Merlin, J., Stechly, L., de Beauce, S., Monte, D., Leteurtre, E., van Seuningen, I., Huet, G. and Pigny, P. (2011). Galectin-3 regulates MUC1 and EGFR cellular distribution and EGFR downstream pathways in pancreatic cancer cells. *Oncogene* **30**, 2514-2525.
Mirzadeh, Z., Merkle, F. T., Soriano-Navarro, M., Garcia-Verdugo, J. M. and Alvarez-Buylla, A. (2008). Neural stem cells confer unique pinwheel architecture to the ventricular surface in neurogenic regions of the adult brain. *Cell Stem Cell* **3**, 265-278.
Mok, S. W., Riemer, C., Madela, K., Hsu, D. K., Liu, F. T., Gultner, S., Heise, I. and Baier, M. (2007). Role of galectin-3 in prion infections of the CNS. *Biochem. Biophys. Res. Commun.* **359**, 672-678.
Moss, J. and Bolam, J. P. (2008). A dopaminergic axon lattice in the striatum and its relationship with cortical and thalamic terminals. *J. Neurosci.* **28**, 11221-11230.
Nam, S. C., Kim, Y., Dryanovski, D., Walker, A., Goings, G., Woolfrey, K., Kang, S. S., Chu, C., Chenn, A., Erdelyi, F. et al. (2007). Dynamic features of postnatal subventricular zone cell motility: a two-photon time-lapse study. *J. Comp. Neurol.* **505**, 190-208.
Ng, L., Bernard, A., Lau, C., Overly, C. C., Dong, H. W., Kuan, C., Pathak, S., Sunkin, S. M., Dang, C., Bohland, J. W. et al. (2009). An anatomic gene expression atlas of the adult mouse brain. *Nat. Neurosci.* **12**, 356-362.
Ochieng, J., Furtak, V. and Lukyanov, P. (2004). Extracellular functions of galectin-3. *Glycoconj. J.* **19**, 527-535.
Ono, K., Tomasiewicz, H., Magnuson, T. and Rutishauser, U. (1994). N-CAM mutation inhibits tangential neuronal migration and is phenocopied by enzymatic removal of polysialic acid. *Neuron* **13**, 595-609.
Partridge, E. A., Le Roy, C., Di Guglielmo, G. M., Pawling, J., Cheung, P., Granovsky, M., Nabi, I. R., Wrana, J. L. and Dennis, J. W. (2004). Regulation of cytokine receptors by Golgi N-glycan processing and endocytosis. *Science* **306**, 120-124.
Pastrana, E., Cheng, L. C. and Doetsch, F. (2009). Simultaneous prospective purification of adult subventricular zone neural stem cells and their progeny. *Proc. Natl. Acad. Sci. USA* **106**, 6387-6392.
Peretto, P., Merighi, A., Fasolo, A. and Bonfanti, L. (1997). Glial tubes in the rostral migratory stream of the adult rat. *Brain Res. Bull.* **42**, 9-21.
Pesheva, P., Kuklinski, S., Schmitz, B. and Probstmeier, R. (1998). Galectin-3 promotes neural cell adhesion and neurite growth. *J. Neurosci. Res.* **54**, 639-654.
Petreanu, L. and Alvarez-Buylla, A. (2002). Maturation and death of adult-born olfactory bulb granule neurons: role of olfaction. *J. Neurosci.* **22**, 6106-6113.
Reichert, F. and Rotshenker, S. (1999). Galectin-3/MAC-2 in experimental allergic encephalomyelitis. *Exp. Neurol.* **160**, 508-514.
Reynolds, B. A. and Weiss, S. (1992). Generation of neurons and astrocytes from isolated cells of the adult mammalian central nervous system. *Science* **255**, 1707-1710.
Rousselot, P., Lois, C. and Alvarez-Buylla, A. (1995). Embryonic (PSA) N-CAM reveals chains of migrating neuroblasts between the lateral ventricle and the olfactory bulb of adult mice. *J. Comp. Neurol.* **351**, 51-61.
Sakaguchi, M., Shingo, T., Shimazaki, T., Okano, H. J., Shiwa, M., Ishibashi, S., Oguro, H., Ninomiya, M., Kadoya, T., Horie, H. et al. (2006). A carbohydrate-binding protein, Galectin-1, promotes proliferation of adult neural stem cells. *Proc. Natl. Acad. Sci. USA* **103**, 7112-7117.
Sato, S. and Nieminen, J. (2004). Seeing strangers or announcing "danger": galectin-3 in two models of innate immunity. *Glycoconj. J.* **19**, 583-591.
Sawamoto, K., Wichterle, H., Gonzalez-Perez, O., Cholfin, J. A., Yamada, M., Spassky, N., Murcia, N. S., Garcia-Verdugo, J. M., Marin, O., Rubenstein, J. L. R. et al. (2006). New neurons follow the flow of cerebrospinal fluid in the adult brain. *Science* **311**, 629-632.
Spassky, N., Merkle, F. T., Flames, N., Tramontin, A. D., Garcia-Verdugo, J. M. and Alvarez-Buylla, A. (2005). Adult ependymal cells are postmitotic and are derived from radial glial cells during embryogenesis. *J. Neurosci.* **25**, 10-18.
Takenaka, Y., Fukumori, T. and Raz, A. (2004). Galectin-3 and metastasis. *Glycoconj. J.* **19**, 543-549.
Tramontin, A. D., Garcia-Verdugo, J. M., Lim, D. A. and Alvarez-Buylla, A. (2003). Postnatal development of radial glia and the ventricular zone (VZ): a continuum of the neural stem cell compartment. *Cereb. Cortex* **13**, 580-587.
Villa-Verde, D. M., Mello-Coelho, V., Lagrota-Candido, J. M., Chammas, R. and Savino, W. (1995). The thymic nurse cell complex: an in vitro model for extracellular matrix-mediated intrathymic T cell migration. *Braz. J. Med. Biol. Res.* **28**, 907-912.
Walther, M., Kuklinski, S., Pesheva, P., Guntinas-Lichius, O., Angelov, D. N., Neiss, W. F., Asou, H. and Probstmeier, R. (2000). Galectin-3 is upregulated in microglial cells in response to ischemic brain lesions, but not to facial nerve axotomy. *J. Neurosci. Res.* **61**, 430-435.
Ward, M. E. and Rao, Y. (2005). Investigations of neuronal migration in the central nervous system. *Methods Mol. Biol.* **294**, 137-156.
Woodworth, A., Pesheva, P., Fiete, D. and Baenziger, J. U. (2004). Neuronal-specific synthesis and glycosylation of tenascin-R. *J. Biol. Chem.* **279**, 10413-10421.
Yan, Y. P., Lang, B. T., Vemuganti, R. and Dempsey, R. J. (2009). Galectin-3 mediates post-ischemic tissue remodeling. *Brain Res.* **1288**, 116-124.
Yang, R. Y., Hsu, D. K. and Liu, F. T. (1996). Expression of galectin-3 modulates T-cell growth and apoptosis. *Proc. Natl. Acad. Sci. USA* **93**, 6737-6742.
Young, K. M., Fogarty, M., Kessaris, N. and Richardson, W. D. (2007). Subventricular zone stem cells are heterogeneous with respect to their embryonic origins and neurogenic fates in the adult olfactory bulb. *J. Neurosci.* **27**, 8286-8296.
Zhao, Q., Barclay, M., Hilkens, J., Guo, X., Barrow, H., Rhodes, J. M. and Yu, L. G. (2010). Interaction between circulating galectin-3 and cancer-associated MUC1 enhances tumour cell homotypic aggregation and prevents anoikis. *Mol. Cancer* **9**, 154.